Iranian Journal of Science and Technology, Transactions of Civil Engineering (2023) 47:3487–3505
https://doi.org/10.1007/s40996-023-01122-w

RESEARCH PAPER

Effects of Soil–Structure Interaction on Performance of Bridges During Earthquakes. Case Study: Integral Abutment Bridge in Pennsylvania, USA

Ali Akbar Firoozi[1] · Maryam Naji[2] · Ali Asghar Firoozi[3]

Received: 15 September 2022 / Accepted: 15 April 2023 / Published online: 18 May 2023

Abstract
Bridges are among the most important transportation elements that may be damaged by earthquakes. An integral abutment bridge (IAB) is a bridge linking the superstructure directly to the substructure. As soil piles, abutments, and superstructures act as a combined system to resist lateral loading on the bridge, soil stiffness has a major impact on load distribution. This research attempts to determine how the structure and soil parameters affect the IABs. The parametric study consists of four variables, namely bridge span (short, medium, and large spans were 18.3, 35.4, and 64.5 m, respectively), backfill height/pressure (3.1, 4.6, and 6.1 m, respectively), stiffness of soil mixture backfills (high, intermediate, and low), and soil density around the piles (high, intermediate, and low). Because of the small width–length ratio of the bridge, a 2D model of an IAB with soil springs around the piles and abutments was developed with finite element software. Findings show that the value of the backfill pressure affects girder axial forces and girder bending moments at the IAB. Also, the stiffness of soil mixture backfills is an important factor to change lateral displacements, while less movement is related to high stiffness of soil mixture backfills with intermediate clay around the pile. It is clear that the maximum axial girder moments at the superstructure generally decrease when the stiffness of the soil mixture behind the abutments and around piles increases, similar to pile deflection and abutment displacements. In addition to maximum abutment, the head moment decreases when abutment backfill is dense and increases when piles are located in hard clay, similar to pile moments. Lastly, dense sand backfill behind abutments is recommended since it decreases pile deflections, pile lateral forces, abutment displacements, abutment head moments, and particularly pile bending moments.

Keywords Seismic analysis · Bridge span · Backfill height · Soil stiffness · Pile

1 Introduction

Integral abutment bridges (IABs) are a form of construction whose superstructures are directly linked to the substructure. They have been used for more than 90 years in many countries and under different seismic conditions (Naji et al. 2020). IABs were introduced in the 1930s in the United States and expanded during the 1960s in many parts of the world (Mahjoubi and Maleki 2020; Dicleli 2016; Khosravikia et al. 2018). As reported by Barghian et al. (2020), the North American Study Tour Report presented several types of abutments: embedded-wall abutments, the full-height frame, spread footings on reinforced earth walls, stub abutments and vertical walls with semi-integral. A bridge receives lateral force due to seismic load and difference in temperature, which affects contraction-related and bridge expansion to soil–structure interaction (SSI) and a variety of materials. In a typical single-span bridge, the substructure and superstructure are integrally constructed, without expansion joints as a rigid connection. This connection transfers most loads from the superstructure to abutments and pile foundations. IABs use relatively flexible pile foundations such as a single pile foundation row to handle superstructure

✉ Ali Akbar Firoozi
firoozia@ub.ac.bw

[1] Department of Civil Engineering, Faculty of Engineering and Technology, University of Botswana, Private Bag. UB0061 Gaborone, Botswana

[2] Department of Civil Engineering, Higher Education Complex of Saravan, Saravan, Iran

[3] Department of Civil Engineering, Shiraz University, Shiraz, Iran

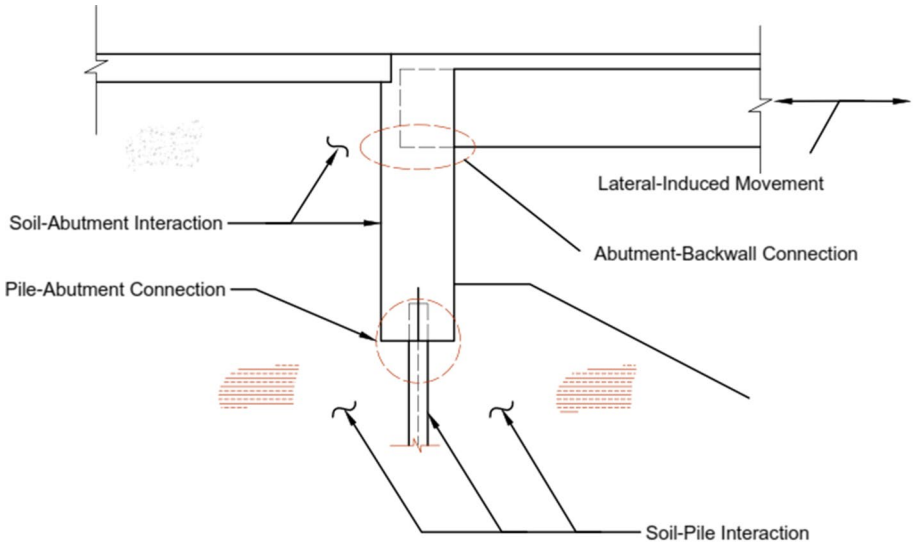

Fig. 1 Component of critical zone in modeling

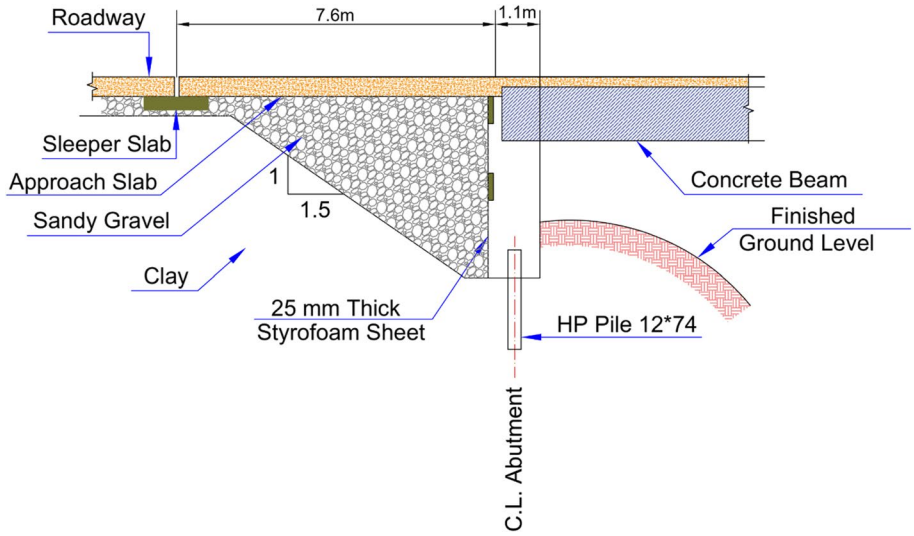

Fig. 2 A section of Bridge 222

expansion and contraction due to laterally induced loads, backfill strain, creep, and shrinkage. However, as soil piles, abutments, and superstructure act as a combined framework to withstand the loading on the bridge, and the SSI properties such as soil stiffness has a significant influence on load distribution (Naji et al. 2020).

Expansion joints and moving bearings at the ends of the deck are replaced by control joints situated at the end of the approach slab, where the structure is not adversely affected by joint leakage. When the foundation has greater flexibility and less resistance to longitudinal displacements, stress from longitudinal forces can be minimized.

IABs have many advantages over conventional bridges. One important benefit of this type of bridge is the removal of expansion joints and bearings (Arsoy et al. 1999; Frosch et al. 2005; Abdel-Fattah and Abdel-Fattah 2019). The most troublesome aspect of bridges is expansion joints, creating numerous serviceability and structural issues. Furthermore, deck length will increase or decrease due to seasonal temperature changes. Since integral bridges are of a continuous unit system, stresses are transferred from the bridge

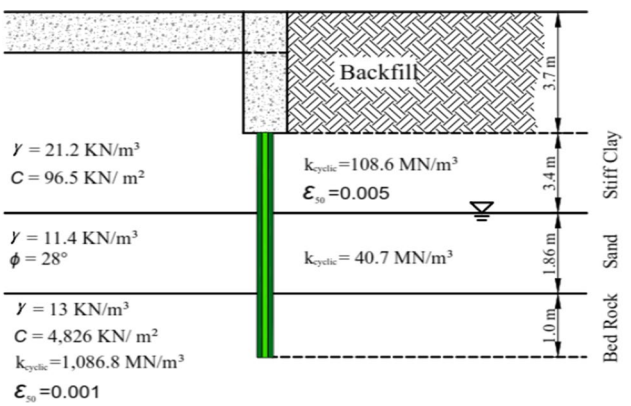

Fig. 3 Soil properties for Bridge 222 at abutment 1 (Pugasap 2006)

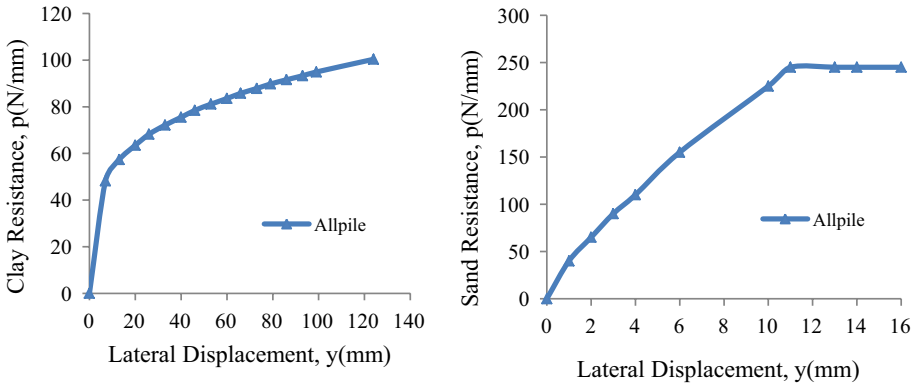

Fig. 4 *p–y* curve for clay and sand

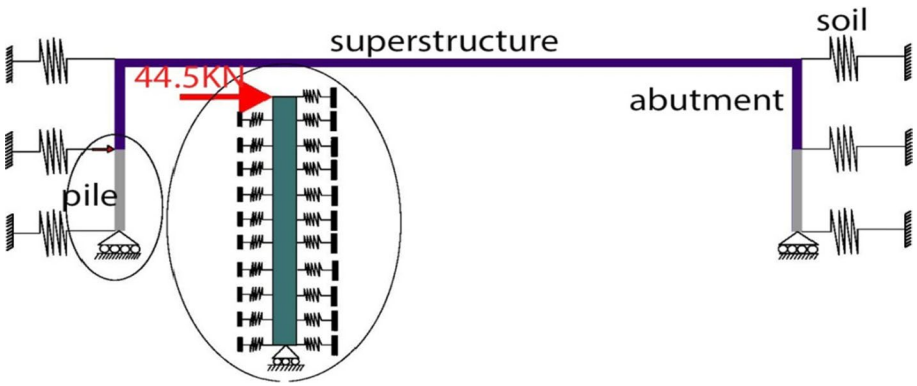

Fig. 5 Single lateral force applied to the head of the pile

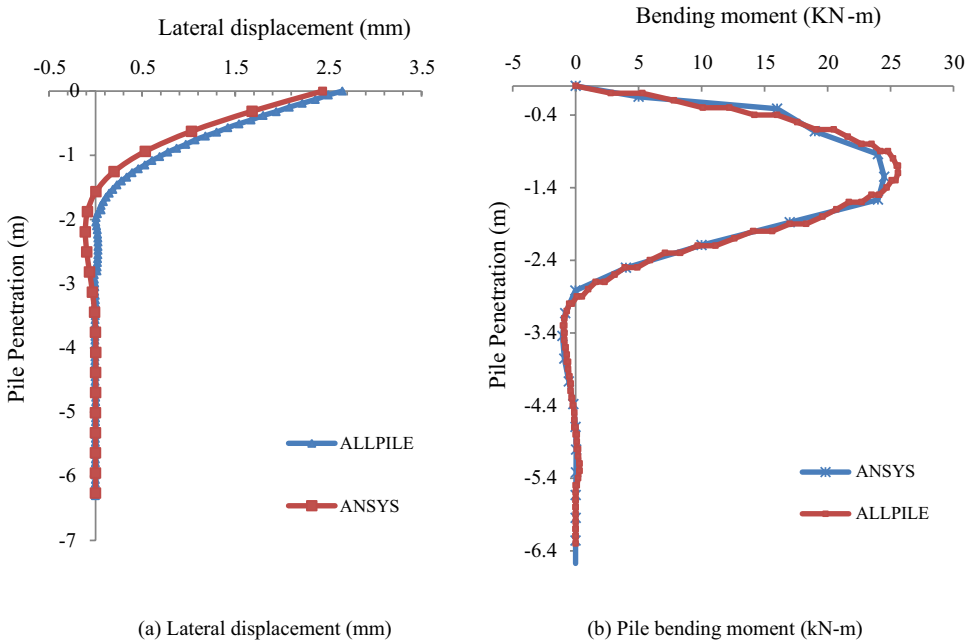

(a) Lateral displacement (mm) (b) Pile bending moment (kN-m)

Fig. 6 Lateral displacement and pile bending moment due to 44.5 kN loads at the pile head

to the soil under the expansion and contraction caused by temperature changes. The amount of force generated in the backfill depends on the expansion and contraction of the bridge. The increase/decrease amount of the deck length is directly related with backfill specifications. Therefore, the reduction or expansion of the bridge and the force created in the backfill are in interact with each other (Perić et al. 2016). SSI at railway bridges with integral abutments studied by Bigelow et al. (2017). They proposed that there are two advantageous aspects of selecting bridges with integral

abutments in general. Firstly, there is an economic factor, because, during their life span, these bridges often tend to be less costly to build, simpler to maintain, and more economical to own. The second key factor concerns the efficiency of the framework. IABs with rigidity properties, which produce load-carrying behavior such as structural frames, have a reduced field moment when subjected to vertical loads, smaller deflections in the mid-span, and smaller abutment rotation angles than traditional bridges with bearings and joints (Bigelow et al. 2017; Tam and Le 2019).

The seismic risk assessment of the bridge systems within the road network is considered to be an important tool for the proper maintenance of the entire network, as well as for the effective mitigation of the direct and indirect socioeconomic losses that may arise as a result of a major earthquake. The most important components of such a highway system are basically bridges since the related uncertainty in the prediction of their fragility directly spreads to the level of the network. Therefore, any simplification of the interaction between earthquake excitation and the dynamic properties of the soil–bridge system in the reliability chain of major the interaction can affect the assessment of the seismic risk of the network (Lesgidis et al. 2017). The numerical simulation of SSI at each pier foundation and abutment-embankment support of the bridge is one of the main elements in the aforementioned reliability chain. It is well known that the nature of SSI is inherently frequency-dependent and, as such, the frequency content of the incoming seismic motion at each bridge support is influenced by the complex dynamic impedance matrix, especially as soil responds inelastically (Saitoh 2007; Pal and Baidya 2018; Makris et al. 1994). Within the context of seismic risk assessment of bridges for both long structures and bridges, various SSI simulation approaches have been implemented. The simulation of the entire soil domain-structure system by a finite element model (FEM) will provide a consistent representation and justification for the semi-infinite soil's dynamic properties and failure mechanisms, allowing the entire system to be evaluated (Sextos et al. 2003).

Field evidence from past earthquakes suggests that the dynamic response can be changed by SSI effects and thus affect the seismic output of bridges. While the effects of SSI have been a subject of interest for researchers, and several detailed solutions are currently available, there is still uncertainty as to the impact of the SSI on the seismic response of bridges, as presented by the conflicting results of numerous research studies (Stefanidou et al. 2017). Collaboration of soil–bridge systems is essentially a case-dependent, multi-parametric problem, and is dependent on various parameters such as type of foundation, structural characteristics, structure-to-soil stiffness, and soil stiffness, as well as frequency, materials, and length and intensity of earthquake ground motion (Nakhaei and Ghannad 2008; Kwon and Elnashai 2006). Consideration of SSI effects requires detailed analytical models, including all major parameters defining the physical problem and all essential structural components of the studied system, given the substantial epistemic and aleatory uncertainty associated with the parameters. During a seismic analysis of bridges, various types of interactions need to be considered, including deck–abutment, soil–foundation–pier, and abutment–embankment, while close coupling between soil conditions and spatially variable soil movements strongly affects longer bridges (Mylonakis et al. 2006; Kotsoglou and Pantazopoulou 2007; Shamsabadi et al. 2005; Taskari and Sextos 2015).

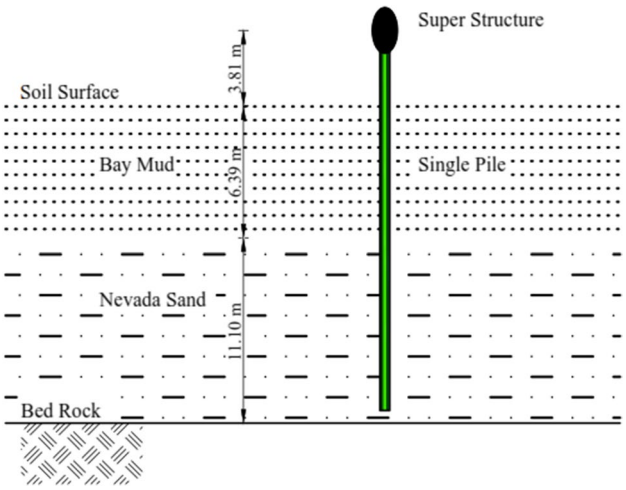

Fig. 7 Profile of soil (Boulanger et al. 1999)

Soil–foundation–pier interaction can consist of soil–pile or pile–soil–pile (i.e., piles-group) interaction for bridges with deep foundations, depending on the method under consideration, while a more simplistic approach based on wave propagation formulations can be adapted for shallow foundations. The influence of SSI on the fragility analysis of bridges has been discussed in several studies (Stefanidou et al. 2017; Lesgidis et al. 2017; Xie and DesRoches 2019). In the case of rigid structures situated on soft soils, these effects are more noticeable, as in the case of bridges with a comparatively light superstructure and a heavy substructure, irrespective of soil stiffness. For seismically isolated bridges and bridge foundations with limited rotational rigidity around their transverse axes, consideration of SSI effects was also found to be significant. Moreover, the significance of the SSI consideration is related to the ratio between the time of the structure and the predominant period at the site and duration of earthquake ground motion, as well as to its

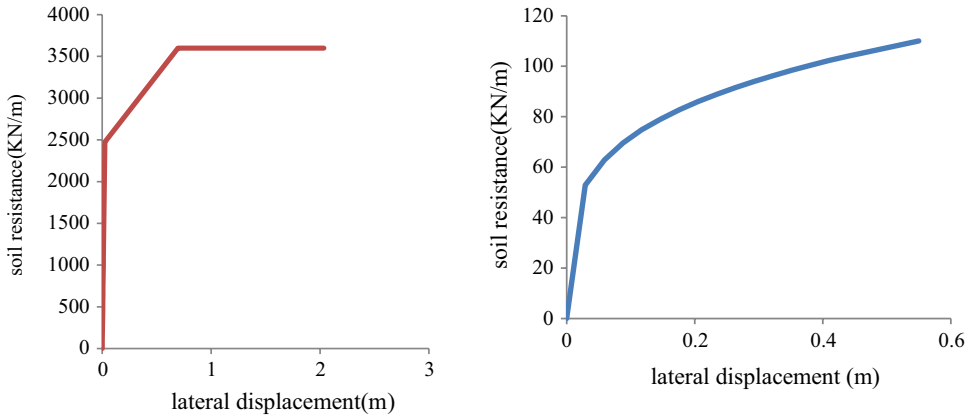

Fig. 8 *p–y* curve for sand and clay

(a) *p-y* curve in 11.2 m depth of sand soil

(b) *p-y* curve in 0.2 m depth of clay soil

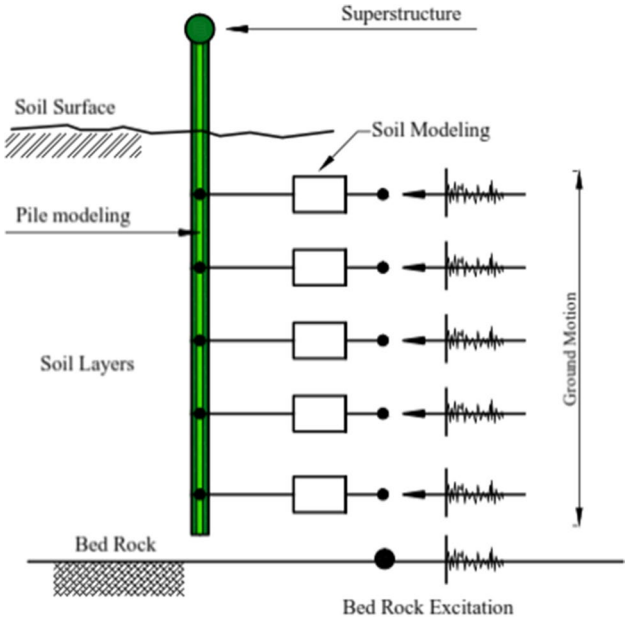

Fig. 9 General view of modeling for nonlinear dynamic loads on the pile

Table 2 Material properties for superstructure models

Bridge	Area, m^2	Modulus of elasticity, MPa	Moment of inertia, m^4	y_b, m
222	4.37	35,536	1.432	1.098

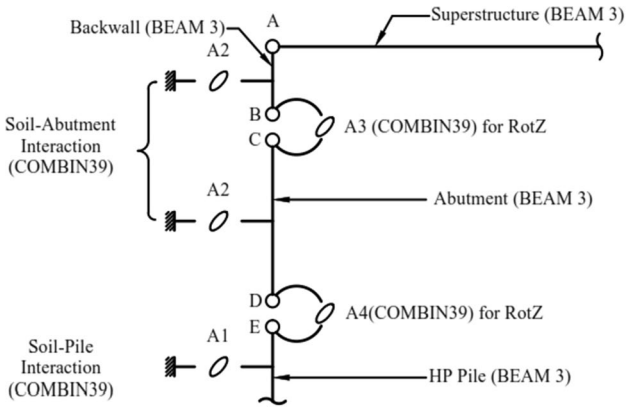

Fig. 10 Schematic representation of substructure modeling

Table 1 Descriptions of the IAB

Bridge	Spans	Span length (m)	Bridge length (m)	Abutment height (m)
222	1	18.9	18.9	2.82

frequency content (Lesgidis et al. 2017, 2018; Rahmani et al. 2018; Lim and Jeong 2018).

In this study, due the small width–length ratio of the bridge, a two-dimensional nonlinear FEM was employed to achieve a parametric study to examine the effect of different parameters on the behavior of the IAB. FEM considered a complete bridge including substructure, superstructure, and soil around it. Seismic analysis of the IAB was conducted on the displacement performance philosophy using nonlinear time history analysis. Such analysis requires the geotechnical engineer's prediction of abutment soils, which is essentially nonlinear with regard to the movement between the bridge structure and backfill. The main objectives of this study were to study the sensitivities and influences of key parameters that significantly affect IAB response and the effects of bridge parameters on IAB performance under seismic loads.

2 Methodology

A complete IAB structure is the superstructure of the bridge that is directly related to its substructure. When subjected to lateral loading, the superstructure and substructure shift towards or away from the backfill, and interaction analysis of the soil base structure is advantageous for the actions of IAB subjected to seismic forces. In this study, 2D FEMs are planned for a single period to investigate the seismic load responses of IABs. As shown in Fig. 1**,** soil–abutment interaction, soil–pile interaction (SPI), connections of abutment back wall, and connections of pile abutment are crucial factors leading to FE model.

The important matter is clarifying the critical sections in a model of an IAB which performs as an integrated structure. A model of a pile is implemented in the bridge to verify FEM. Then, *p–y* curves of the pile at various heights below the ground are measured. The pile model is then formulated in FE software (i.e., ANSYS), and the same lateral forces are installed on the pile. The next step is to verify the model

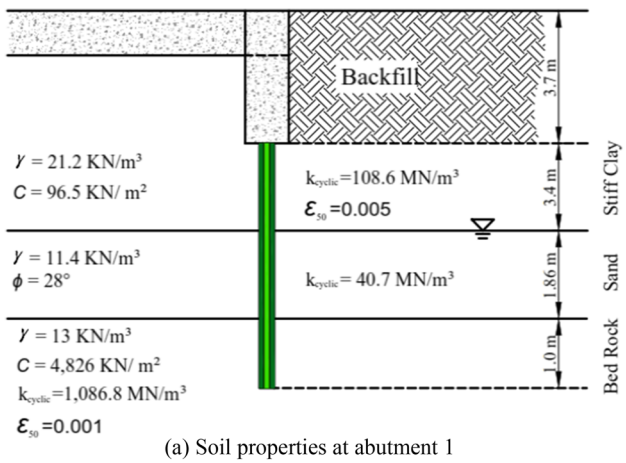

(a) Soil properties at abutment 1

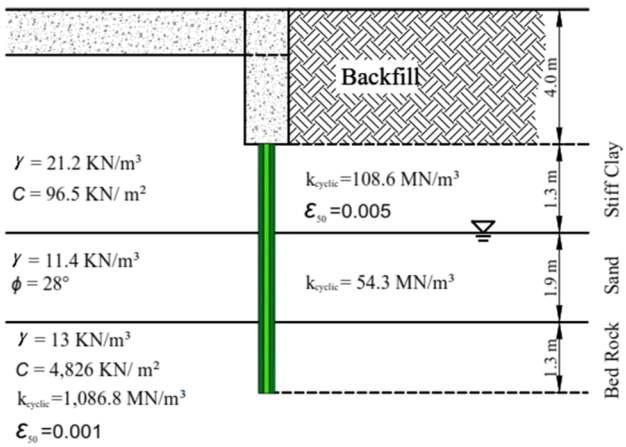

(b) Soil properties at abutment 2

Fig. 11 Soil properties for Bridge 222 (Pugasap 2006)

formulation procedure under dynamic load. Since the seismic behavior of an IAB is the focus of the present study and loading is performed under a dynamic load, it is necessary to implement a method to formulate a soil model which could be effective for the model under a dynamic load whose precision can be measured with high probability. The model formulation of the back wall follows the same procedure. The connection between the abutment and the back wall is a very critical part of modeling, which is the next critical stage of model formulation. Therefore, the $(M-\phi)$ diagram is applied to draw the $(M-\theta)$ diagram which is the necessary for model formulation of nonlinear behavior of connections.

Soil–pile (SP) and soil–abutment interactions, known as SSIs, are related to geotechnical behavior, while abutment back wall and pile abutment connections are related to the yielding of structural connections. SSI is generally a more influential parameter than the yielding of structural connections because soil exhibits nonlinear and hysteretic behavior even over a small range of deformations. In addition, the yielding of structural connections may never occur in a lifetime of bridge structures, if properly designed. The classical *p–y* curve technique is assumed to deliver a load-deformation curve of laterally loaded SPI behaviors. *p–y* curves are generated using the COM624P computer program developed by Wang and Reese (1993). The *p–y* curve method is an SSI analysis method based on the modulus of subgrade reaction. The *p–y* curve method was originally developed using finite difference techniques. The substitution of nonlinear *p–y* curve springs in the governing equation was done instead of using a traditional linear Winkler spring. An iterative solver was implemented to achieve a numerical solution in this transition. Although a nonlinear spring generated from the *p–y* curve method is considered uncoupled, validation of this method was performed against full-scale experiments explicitly to include a continuum effect (Wang and Reese 1993). A series of *p–y* curves along the pile length are generated by pile analysis software (i.e., AllPile (AP)). AllPile is a Windows-based analysis program that can handle most types of piles, from steel pipes, HP piles and precast concrete piles to drilled shafts and shallow foundations. Lateral analysis in AP software utilizes the finite difference method for the modeling of SSI. In lateral loading, the pile shaft deflects and exerts pressure on the adjacent soils, resulting in the generating of lateral resistance (pressure) between soils and the pile. By integrating lateral pressure, shear, moment, rotation, and deflection, an analysis of the pile and soil interaction and behavior is obtained. For validation of FE software (i.e., ANSYS) and AP software, one pile of implemented IAB is chosen and modeled with FE software by *p–y* curves taken from AP software; then the output of FE and AP is compared. Bridge 222, the IAB selected for modeling which is located in Pennsylvania in the United States and the implemented plan is shown in Fig. 2.

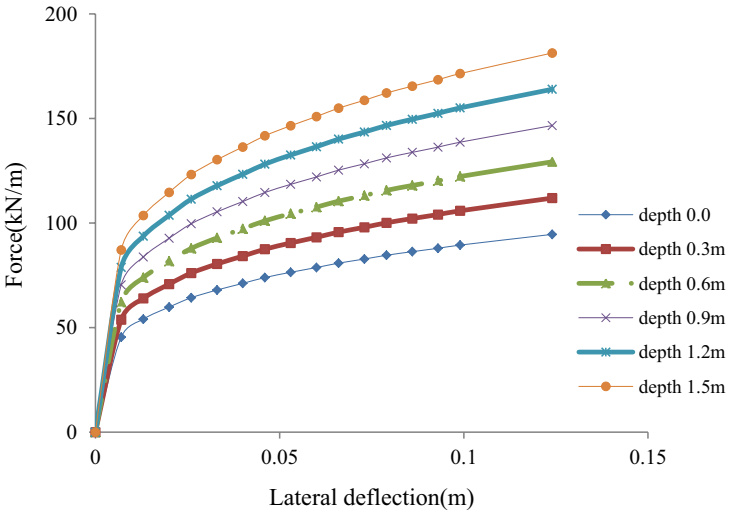

(a) *p-y* curve for stiff clay

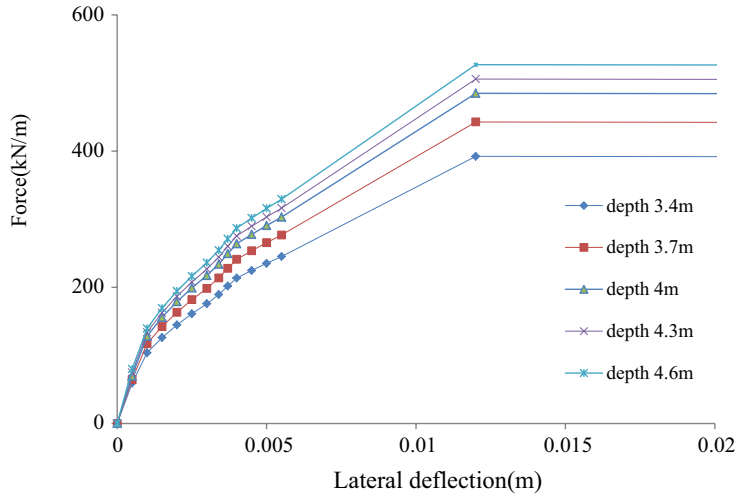

(b) *p-y* curve for sand

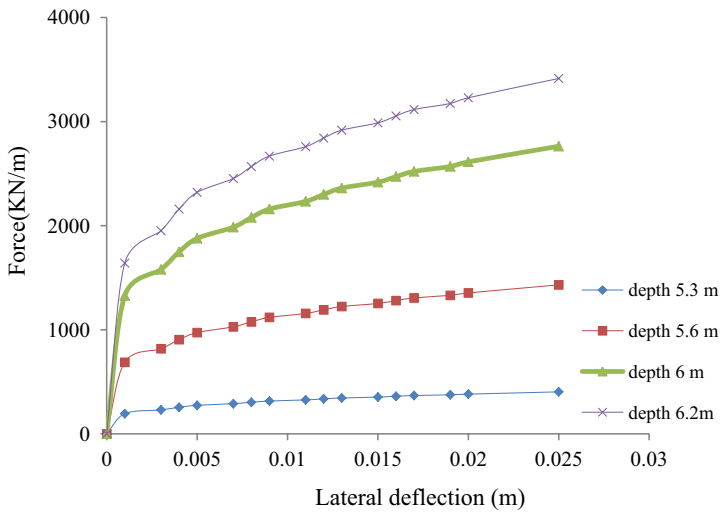

(c) *p-y* curve for bedrock

Fig. 12 *p–y* curves for the pile at abutment 1

Table 3 Material properties for substructure models

Bridge	Components	Modulus of elasticity Mpa	Area m^2	Moment of inertia m^4
222	Abutment	21,760	16.80	2.081
	Back wall	25,124	16.80	2.081
	Pile (abutment1)	200,000	0.155	8.52E-4
	Pile (abutment2)	200,000	0.127	6.97E-4

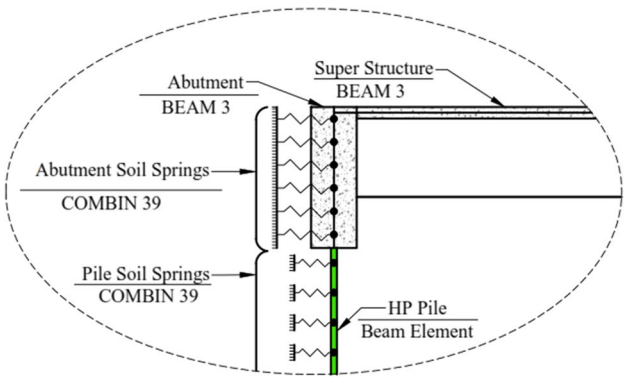

Fig. 13 Soil–structure (pile, abutment, back wall) interaction view

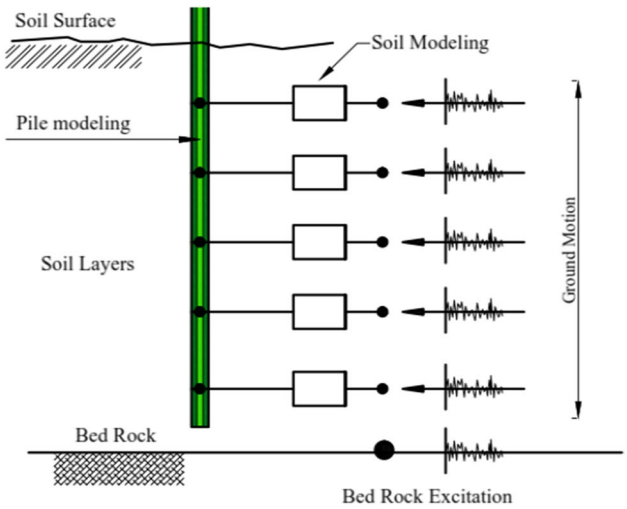

Fig. 14 Applied loads in FE software

Soil parameters were obtained from the soil profile of Bridge 222 for clay above the water table and sand, respectively, as illustrated in Fig. 3. Samples of *p–y* curves generated by AP software are presented in Fig. 4.

The multilinear curves represent a nonlinear soil spring in FE software. The COMBIN39 element type was adopted as an appropriate nonlinear one-dimensional element in FE. A lateral force of 44.5 kN, which produces a working range of actual pile movements of Bridge 222 and a free-end boundary condition was applied at the pile head, as displayed in Fig. 5. The maximum pile moment occurs at the top of the pile. The value is dependent on pile deformations and abutment rotation. Pile behavior can be considered similar to a cantilevered member with a free end at the first point of inflection in the pile and partial release of end moment restraint at the pile top depending on abutment rotation, with soil-springs attached along this length (Shedge and Kumar 2022; Salman and Issa 2019; Abdelrahman et al. 2018; Xie et al. 2017; Zhang et al. 2008; Civjan et al. 2007; Teguh et al. 2006). Both AP and FE software display highly similar response to the lateral forces on the pile head (Fig. 6). Maximum displacement was 2.44 mm by FE software and 2.65 mm by AP software, while the maximum moment was 24.5 kN·m and 25.6 kN·m by FE and AP software, respectively. The FEM predictions of pile behavior were similar to AP, with percentage differences of 8% and 8.5%, for a maximum displacement and maximum moment, respectively. Element length in the FE pile model was relatively coarse (33 mm) compared to the length used in AP (30 mm). Therefore, some small differences in moments at a depth of approximately 3 m are expected to appear, where a short distance between two adjacent inflection points occurs. It is not possible to select elements with the same length because element length in AP is automatically determined by software, but in FE, several extra nodes with minor element length are generated because the user limits the coordinates of nodes. This increases error probability; hence, it is recommended to avoid such element length difference.

The dynamic response of piles in bridges with pile foundation is a function of the characteristics of the loading, dynamic pile–soil interaction behavior and dynamic characteristics of the piles structural system. The seismic soil–pile structure interaction analysis is the primary

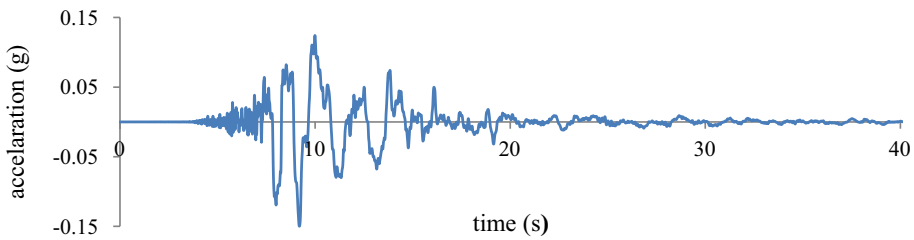

Fig. 15 Time history accelerations in the soil profile during the event of 0.15 g at 2 m depth

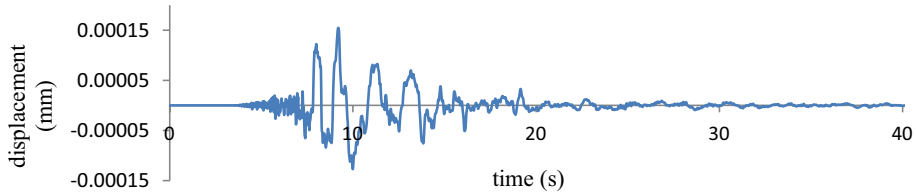

Fig. 16 Time history displacement in the soil profile during the event of 0.15 g at 2 m depth

Table 4 Maximum abutment displacements

Case	Abutment 1 (mm)		Abutment 2 (mm)	
	Top	Bottom	Top	Bottom
Bridge 222	0.397	−6	−0.397	6

Table 5 Moment of pile head and girder axial forces

Case	Moment of pile head (kN-m)	Girder axial force (kN)
Bridge 222	23	154

Table 6 Soil properties

Property	Units	High	Intermediate	Low
Clay density	kN/m^3	22	19	16
Elastic modulus	MN/m^2	353	271	190
ε_{50}	mm	0.13	0.20	0.25

step in evaluating the seismic behavior of pile-supported structures. The pile–soil interaction problem when an earthquake occurs with its accompanying stresses is one of the most significant sources of nonlinear dynamic response analysis of bridges, which has gained attention in recent years and several studies have investigated the characteristics of ground motion input and the mechanism of pile–soil interaction to determine seismic load design for structures that are pile-supported (Shamsi et al 2021; Souri et al. 2022; Li et al. 2022). *p–y* analysis is used to analyze the dynamic response of piles and should allow for a variety of soil properties with depth, nonlinear soil behavior, nonlinear behavior of pile–soil interfaces and energy dissipation through hysteretic damping. The method of validating the reliability of *p–y* analysis followed in this study is evaluated with an experimental test that involves a series of dynamic centrifuge model tests of pile-supported structures in the soft ground followed by an evaluation of the capability of the *p–y* analysis method, which is done to obtain a reliable picture of the SPI effects. Experiments were conducted by Boulanger et al. (1999) at the University of California, Davis, using a large servo-hydraulic shaking table. The profile of the soil consisted of two horizontal layers of soil with a lower layer of fine, evenly graded Nevada sand, 11.10 m thick with C_u equal to 1.5 and D_{50} equal to 15 mm, where C_u is the ultimate shear stress of soil and D_{50} is the relative density in average particle size. The sand dryness density was 1.66 mg/m^3 at a relative density (D_r) of 75–80%. The upper layer was of reconstituted bay mud 6.39 m thick with a plasticity index of 48%.

The single pile-supported system employed in this test was a 670 mm steel pipe with 19 mm wall thickness and a total length of 20.57 m and a superstructure with a mass of 49,100 kg connected to an extension of the pile of 3.81 m above the ground surface. Figure 7 presents the single pile–soil profile and superstructure systems. The pile structure was separated into 12 elastic–plastic beam elements, with 11 elements below the soil surface and one element above ground. Each sub-ground pile node was linked to a set of parallel nonlinear *p–y* elements on each side of the pile modeled with COMBIN39 for nonlinear springs. Interface elements were employed to join the pile and soil nodes at each level and on each side of the pile. Acceleration time histories at various soil layers derived from the free field site response analyses using the EERA program.

EERA is an implementation of the equivalent linear concept of earthquake site response analysis that is an add-on in Excel. EERA input was used to define the earthquake acceleration time history as well as the geometry and properties of the soil profile. With this application, it is possible to obtain the time history acceleration and displacement in different layers for that the user chose. At this stage of study, this application software is used to determine the desirable time history analysis.

The soil profile is defined in AP software and then a *p–y* curve is created for the pile dimensions in various heights of soil. As is shown in Fig. 8, the soil profile at the 0.2 m height is composed of clay, and at the 11.2 m height it is made up of sand with certain specifications which were used in the experiment. Furthermore, the ground movement of the soil layers was measured due to earthquake excitations performed on the bedrock in site response analysis. The results of this free-field analysis (acceleration or displacement time histories at different soil layers) are shown in Fig. 9 and become the input excitation at the FEM support nodes.

Table 7 Parametric study cases

Case ID	Bridge span (*L*) m	Backfill height (*H*) m	Stiffness of soil mixture backfills (*B*)	Clay stiffness around piles (*P*)
1	18.3	3.0	High (*h*)	High (*h*)
2				Intermediate (*i*)
3				Low (*l*)
4			Intermediate (*i*)	*h*
5				*i*
6				*l*
7			Low (*l*)	*h*
8				*i*
9				*l*
10		4.6	*h*	*h*
11				*i*
12				*l*
13			*i*	*h*
14				*i*
15				*l*
16			*l*	*h*
17				*i*
18				*l*
19		6.1	*h*	*h*
20				*i*
21				*l*
22			*i*	*h*
23				*i*
24				*l*
25			*l*	*h*
26				*i*
27				*l*
28	35.4	3.0	*h*	*h*
29				*i*
30				*l*
31			*i*	*h*
32				*i*
33				*l*
34			*l*	*h*
35				*i*
36				*l*
37		4.6	*h*	*h*
38				*i*
39				*l*
40			*i*	*h*
41				*i*
42				*l*
43			*l*	*h*
44				*i*
45				*l*
46		6.1	*h*	*h*
47				*i*
78				*l*
49			*i*	*h*
50				*i*
51				*l*
52			*l*	*h*
53				*i*
54				*l*

Table 7 (continued)

Case ID	Bridge span (*L*) m	Backfill height (*H*) m	Stiffness of soil mixture backfills (*B*)	Clay stiffness around piles (*P*)
55	64.5	3.0	*h*	*h*
56				*i*
57				*l*
58			*i*	*h*
59				*i*
60				*l*
61			*l*	*h*
62				*i*
63				*l*
64		4.6	*h*	*h*
65				*i*
66				*l*
67			*i*	*h*
68				*i*
69				*l*
70			*l*	*h*
71				*i*
72				*l*
73		6.1	*h*	*h*
74				*i*
75				*l*
76			*i*	*h*
77				*i*
78				*l*
79			*l*	*h*
80				*i*
81				*l*

3 FE Modeling

The bridge discussed in this study is a single-span bridge on the I-99 extension in Pennsylvania Bridge 222 (Fig. 2) and includes element types, mesh sizes, section properties, and material properties for component elements. A composite slab, abutment, girder section, back wall, and piles for the bridge were combined and modeled using the ANSYS BEAM3 element, which is a uniaxial element capable of tension, compression and bending. Each node of the element possesses three degrees of freedom: translations in the nodal *x* and *y* directions and rotation about the nodal *z*-axis. Table 1 shows a short description of the structure of the instrumented integral abutment bridges of four prescribed concrete girders with a cast-in-place deck and without angle at the end on both abutments. The abutments are supported by a single row of weak axis-oriented steel piles by HP12×74. An ANSYS BEAM3 element was used to combine a composite slab and four girder sections. This beam member was subdivided into 10 pieces, and all were located on a composite elastic neutral axis. The elastic modulus of girders was used as a reference modulus so that the slab and parapet widths were transformed using corresponding modulus ratios. AASHTO LRFD was used to determine a concrete modulus of elasticity based on a concrete girder strength of 55.2 MPa. Table 2 presents the material properties of the superstructure.

As shown in Fig. 10, three parts including: A_1 (SPI), A_2 (soil–abutment interaction) and A_3 (abutment back wall connections), respectively, were applied to the bridge components. A_1 hysteresis element shows that a nonlinear spring was connected to two adjacent pile elements through a single node to represent SPI. A single degree of freedom U_X was used for these elements, as we were only interested in the longitudinal movement. Similar to the A_1 case, the A_2 element was connected to two adjacent abutment elements inside the line segment *C–D* and two back wall elements inside segment *A–B*, through a single node to represent soil–abutment interaction. One degree of freedom U_X was enabled for each A_2 element with an element spacing of approximately 0.3 m. Unlike the A_2 case, a single A_3 element was used to connect the bottom of the back wall component (node B) to the top of the abutment component (node C). One degree of freedom in the *z* direction was applied for

Table 8 Time history results in the critical locations

ID Case	Pile head lateral force F_P (kN)	Pile head displacement Δ_P (mm)	Pile head moment M_P (kN-m)	Girder axial force P_g (kN)	Abutment moment M_{ge} (kN-m)
1	12.5	−1.75	37.9	−345.5	−689.3
2	10.5	−1.54	35.7	−351.3	−633.1
3	7.8	−7.68	32.8	218.3	−597.9
28	−30.8	5.03	−49.2	−437.4	−815.0
29	35.5	8.7	−48.8	−441.1	−869.4
30	25.9	−4.9	38.5	367.1	948.4
55	−45.1	0.5	−67.6	−528.4	1235.2
56	−40.6	0.4	−55.249	−535.5	1357.2
57	−37.2	0.2	−53.4	−587.3	−987.1

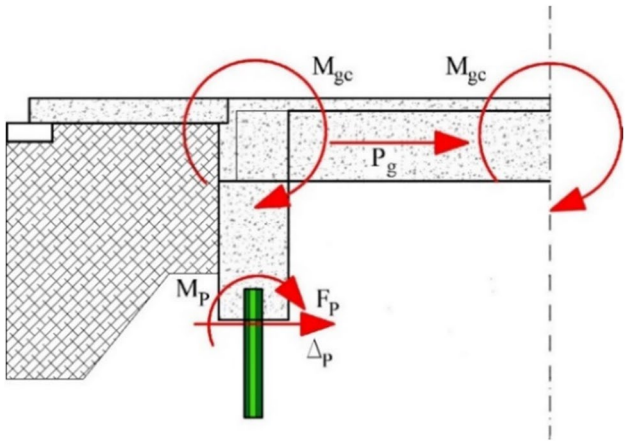

Fig. 17 Critical locations

this case to represent the hysteretic behavior of the abutment back wall connection. For the other degrees of freedom, U_X and, U_Y a coupling of nodes B and C were employed. It is noted that nodes B and C overlap. Properties of the A_1 element were obtained primarily from *p–y* curves, generated by using AP. These properties depended on depth, embankment slope, soil overburden, pile stiffness, and soil properties. Figure 11 presents diagrams of soil profiles and properties for two abutments of the bridge on each side of the bridge. As it is shown, the soil is composed of three layers: stiff clay, sand, and bedrock. *p–y* curve specifications are related to characteristics of soil such as stiffness and overburden. As it was discussed earlier, the length of the pile element is defined as 0.3 m in FE software. Figure 12 shows the *p–y* curve at different levels in increments of 0.3 m.

3.1 Material Properties of Substructure

All material properties of the instrumented bridge are shown in Table 3 and Fig. 13 shows soil backfill interaction modeling.

3.2 Loading

The bridge is located in Pennsylvania, United States, which is a moderate seismic zone and has a PGA of 0.15 g. As it is clearly seen in Fig. 14, the loading in FE time history of the lateral displacement is applied on each node. Nonlinear time history analyses are conducted utilizing the scaled component of the Kobe earthquake to apply to the longitudinal direction of the bridge. Figure 15 indicates the time history of accelerations at a height of 2 m below the surface of the soil profile and Fig. 16 shows its equivalent displacement. The largest lateral displacements above and below the abutment walls during the time history analysis are presented in Table 4 for abutments, showing how generally the maximum wall lateral displacements are greater at the bottom and well matched with the pile deflection. Consequently, all lateral and longitudinal loads applied to the superstructure of the bridges are transmitted directly to abutment embankments. Furthermore, the highest positive and negative moments in the head of piles for the duration of the time history analysis are presented in Table 5. It appears that there is a normal reduction in the girder moments along the bridge within the span due to the stiffness of the soil at the back of the abutment and in the area surrounding the piles, like the pile deflection and abutment displacement. Table 6 presents the high and low soil stiffness properties of clay.

4 Results and Discussion

This study performed 81 sets of parametric investigation of IABs using a two-dimensional numerical FEM. The considered parameters include bridge span, backfill height, backfill stiffness, and clay stiffness around the pile listed in Table 7. The specific locations of critical responses are shown in Fig. 17.

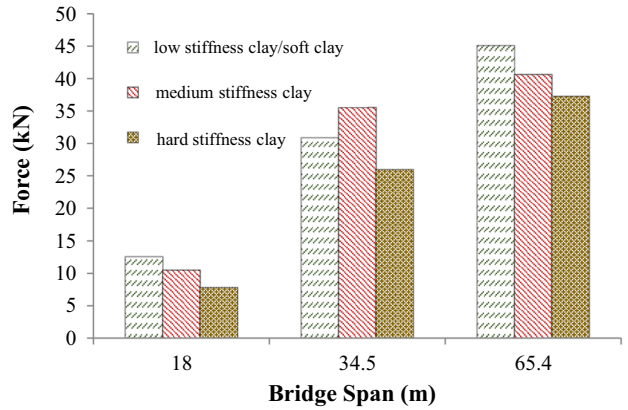

(a) The absolute value of lateral forces

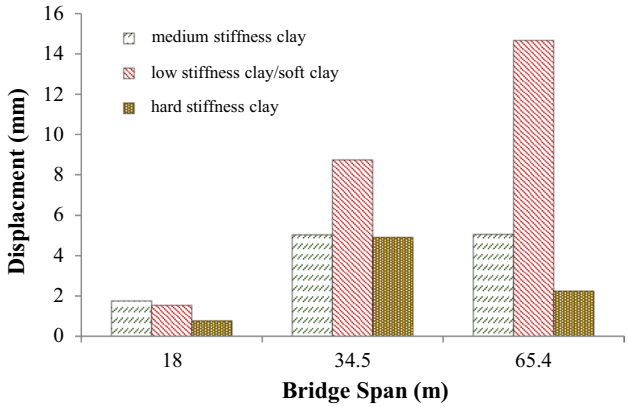

(b) The absolute value of displacements

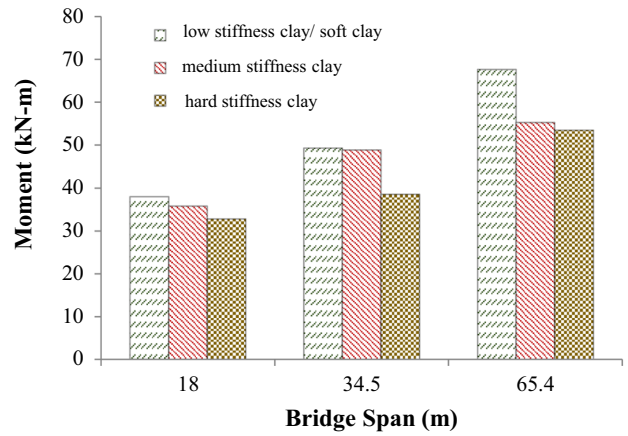

(c) The absolute value of pile head moments

Fig. 18 Effects of bridge span on critical response with consideration soil stiffness around the pile

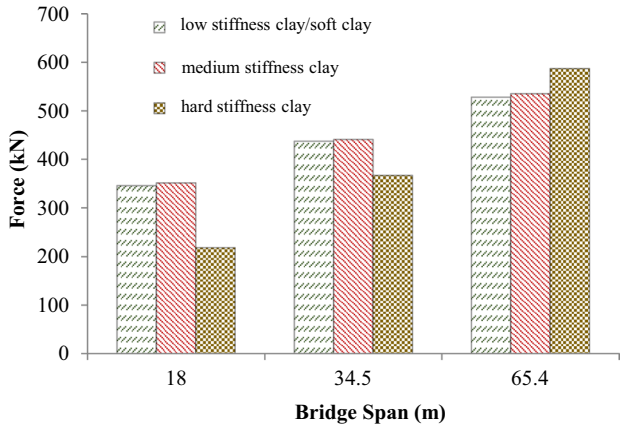

(d) The absolute value of girder axial forces

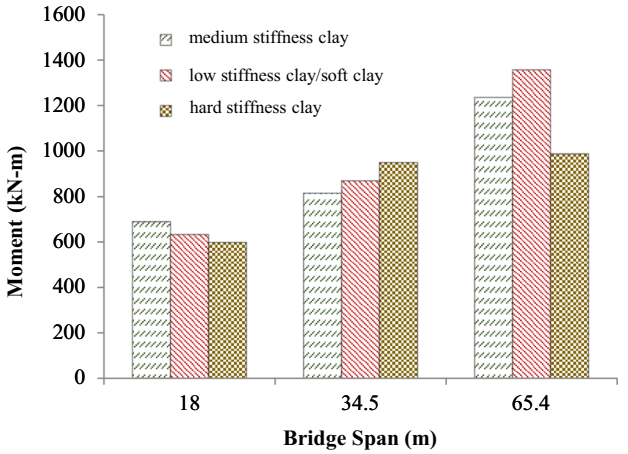

(e) The absolute value of abutment head moments

Fig. 18 (continued)

Table 9 ID Cases for back wall height effect

ID case	Bridge span	Soil stiffness clay
1	18.3	High
10	18.3	Intermediate
19	18.3	low
28	34.5	High
37	34.5	Intermediate
46	34.5	low
55	65.4	High
64	65.4	Intermediate
73	65.4	low

4.1 Effects of Bridge Span on Critical Response

The bridge span shows significant effects on the pile lateral force (F_P); for 18.3, 34.5, and 65.4 m, IABs with abutment height of 3.0 m were found to be 12, 30, and 45 kN with high stiffness backfill, respectively. As the bridge span was increased, the pile bending moment increased substantially as well. The maximum average positive moment (M_P) for the 18.3 m span was 32.13 kN·m, whereas for the 34.5 m span it was 42.38 kN·m, and lastly the 65.4 m span results showed 71.13 kN·m. The maximum average negative moment (M_P) for the 18.3 m span was −30.5 kN·m, and for the 34.5 m

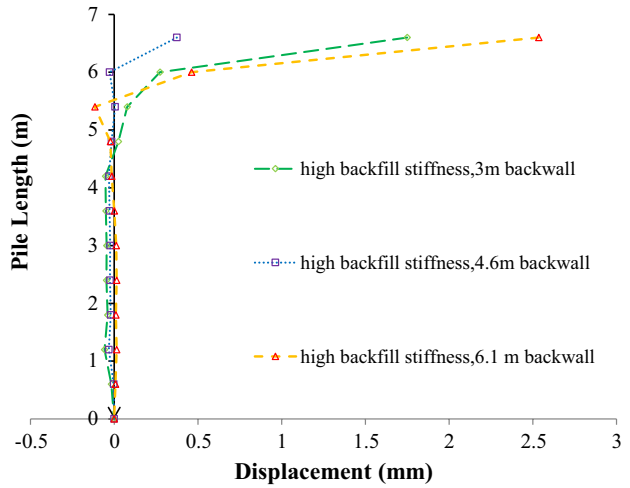

(a) 18.3 m span

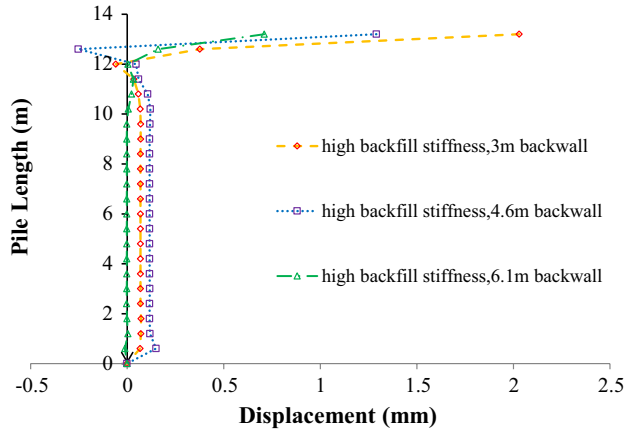

(b) 34.5 m span

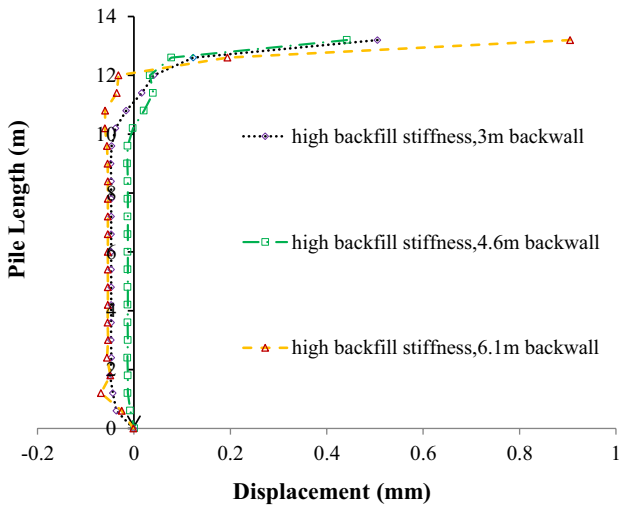

(c) 65.4 m span

Fig. 19 Lateral displacements for pile 1

span it was −42.38 kN·m, while for the 65.4 m span it was −79.13 kN·m. With increases in bridge span, both compressive and tensile girder axial forces (P_g) increased considerably. The maximum average compressive girder axial force found was 389.7 kN and 795.1 kN for spans of 18.3 m and 65.4 m, respectively. The maximum average tensile girder axial force was 250.0 kN and 522.1 kN with a span of 18.3 m and 65.4 m, respectively. As the bridge span increases, both positive and negative girder bending moment at the abutment (M_{ge}) increase significantly. Table 8 summarizes the analyses and Fig. 18 displays the absolute value of outputs relative to the seismic load applied in the longitudinal direction as parametric modeling cases considered by bridge span including the stiffness of the soil around the pile. For instance, when a span of 18.3 m is subjected to ground motion, the maximum lateral force in the longitudinal direction is obtained as 12.5 kN for the case where the stiffness of the soil around the pile is high. However, for spans of 34.5 and 65.4 m using the same ground motion and scales and including the SPI performance in the structural models, the maximum lateral forces were 35.5 and 45.1 kN, respectively. The differences between the maximum displacements found from the spans of 18.3, 34.5, and 65.4 m were 30% and 24%, respectively, as shown in Fig. 18d.

4.2 Effects of Backfill Materials on Critical Response

In a seismic case, the nonlinear force–displacement capability of the bridge abutment is built primarily from mobilized passive pressure behind the back wall of the abutment. Therefore, proper abutment backfill system modeling is important and allowance for nonlinear stiffness must be made. To determine the effect of backfill height on the critical response of the bridge after time history analysis, we selected three levels of height as shown in Table 9. For the domain of backfill height, all backfill stiffness behind the abutment selected high density as soil parameters described in Table 7. This is because of the lateral displacement revealed by the change in the backfill height of the bridge. Time history analysis was applied in all cases and pile displacements (Δ_P) for three spans (i.e., 18.3 m, 34.5 m, and 65.4 m) and results presented in Fig. 19. The variables selected in the above tables were bridge span and backfill height changes in the three levels. In Fig. 19a, three bridges with the same span of 18.3 m were analyzed. Considering the conditions of equality to the stiffness of backfill with high-stiffness sand behind the abutment, abutment height has no significant influence on the lateral displacements (Δ_P). This process is repeated in Fig. 19b and c. By changing the height of the abutment with the accompanying span of the bridge, the structural stiffness increased, but this factor is not related to the lateral displacements.

Table 10 Time history results in critical location

ID case	Pile head lateral force F_P (kN)	Pile head displacement Δ_P (mm)	Pile head moment M_P (kN·m)	Girder axial force P_g (kN)	Abutment moment M_{ge} (kN·m)
1	12.5	−1.75	37.9	−345.5	−689.3
10	13.3	0.37	28.9	−310.6	−55.4
19	11.0	2.54	−32.6	347.5	−29.0
28	−30.8	5.03	−49.2	−437.4	−815.0
37	26.6	−1.3	42.7	323.8	472.1
46	−23.3	7.10	−41.4	−251.0	223.1
55	−45.1	0.5	−67.6	−528.4	1235.2
64	33.9	−0.44	71.2	723.3	515.0
73	−43.9	0.9	−91.7	831.6	213.3

Table 11 Time history results considering backfill stiffness effect

ID case	Pile head lateral force F_P (kN)	Pile head displacement Δ_P (mm)	Pile head moment M_P (kN·m)	Girder axial force P_g (kN)	Abutment moment M_{ge} (kN·m)
1	12.5	−1.7	37.9	−345.5	−689.3
5	11.0	4.4	35.8	−23.2	−199.8
9	−6.6	−5.9	30.6	−180.3	−54.7
28	5.03	5.03	−49.2	−437.4	−815.0
32	9.2	−0.8	34.7	−391.2	−583.8
36	−22.2	7.3	40.5	426.5	476.0
55	−45.1	0.505	−67.6	−528.4	1235.2
59	41.7	−0.33	64.7	817.6	675.0
63	33.3	7.3	68.6	514.4	−220.8

The backfill height influences pile lateral forces (F_P). The average pile lateral force for 18.3 m span and 3.0 m height of backfill was 9.54 kN, for 4.6 m it was 12.16 kN, and for 6.1 m it was 13 kN. In addition, backfill height does not influence pile bending moments (M_P). The average change in pile moment between 3.0 and 6.1 m was −6.37 kN·m. However, the increase in backfill height led to larger displacement when the soil stiffness around the pile was low. The results of the time history analysis are presented in Table 10. Backfill height significantly influences girder axial forces (P_g). The average increase in tensile and compressive girder axial forces (P_g) between the considered cases with 18.3 m and 65.4 m was 410 kN and −165 kN, respectively. An increase of backfill height significantly decreases tensile axial force (P_g), while backfill height has little influence on compressive axial forces. The maximum average tensile girder axial force reduction between 3.0 and 6.1 m was −325 kN. Also, backfill height affected the girder bending moments at the abutment (M_{ge}). An increase of backfill height significantly decreases the positive girder bending moment at the abutment. The maximum average positive moment decreased between 3.0 and 6.1 m and was 482 kN·m for the span of 18.3 m, while the average negative girder moment was 233 kN·m for the span bridge. Figure 20 shows the absolute values of outputs relative to the seismic load applied in the longitudinal direction as parametric modeling cases considered by backfill height including the soil stiffness around the pile. Figure 20 shows that simplification of the structural model leads to a substantial clarification of the full value of the IAB. For example, when the back wall height is 3.0 m subjected to ground motion, the maximum lateral force in the longitudinal direction is 30.8 kN for the case where the soil stiffness around the pile is high. However, for back wall heights of 4.6 and 6.1 m analyzed using the same ground motion and scales and including the SPI behavior in structural models, the maximum lateral forces obtained were 40.0 and 41.7 kN, respectively. The changes between maximum displacements found from 3.0, 4.6, and 6.1 m heights of backfill were 37.8% and 85.6%, respectively (Fig. 20b).

5 Summary of Backfill Height

The results show that backfill height does not have a significant impact on pile lateral forces and pile bending moments (M_P). Backfill height significantly affects girder axial forces.

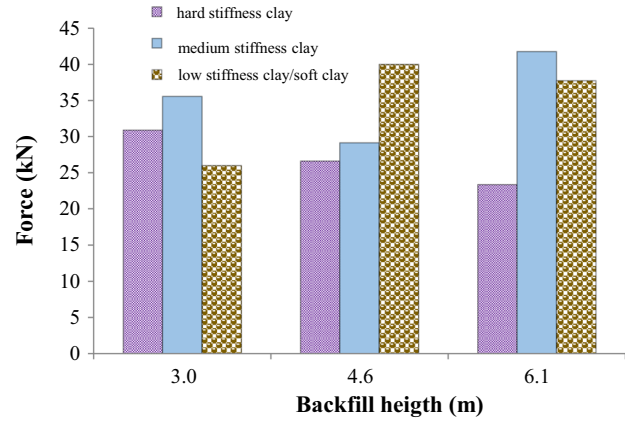

(a) The absolute value of lateral forces

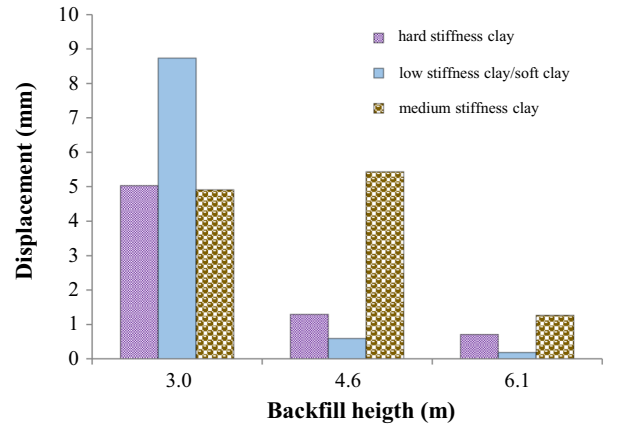

(b) The absolute value of displacements

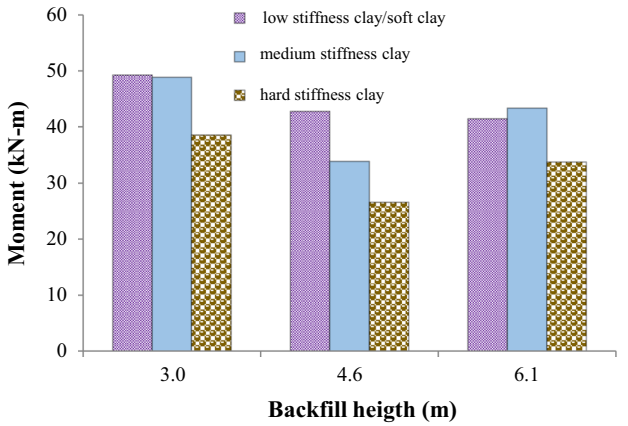

(c) The absolute value of pile head moments

Fig. 20 Effects of soil stiffness on different parameters (lateral forces, displacements, pile head moments, girder axial forces, and abutment head moment)

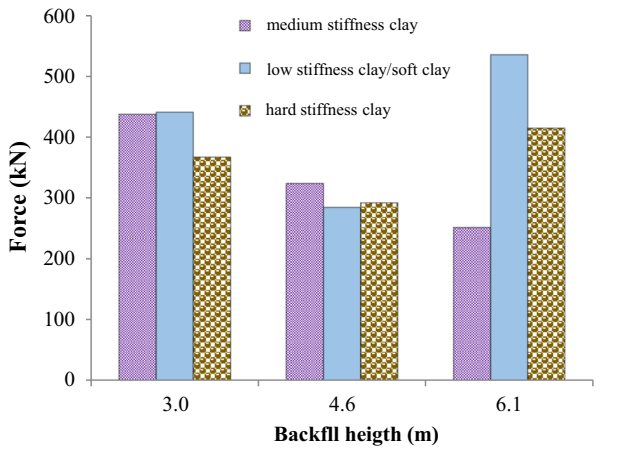

(d) The absolute value of girder axial forces

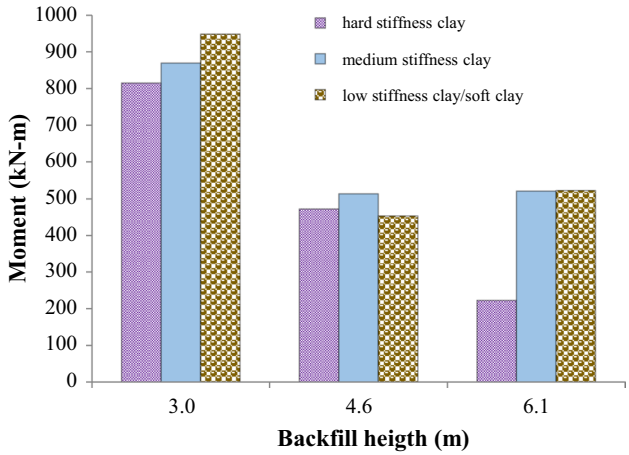

(e) The absolute value of abutment head moments

Fig. 20 (continued)

An increase in backfill height decreases tensile axial forces (P_g), while it shows little effect on the compressive axial forces. Backfill height significantly influences the girder bending moments. The results of the time history analysis are shown in Table 11. The maximum average compressive girder axial force increased between low-stiffness and high-stiffness clay, and it was 73.95 kN. The average increase in tensile girder axial forces was 123.41 kN. The superstructure forms a convex curve during bridge expansion while it forms a concave curve during bridge contraction. This shape formation is more obvious in single-span bridges.

Figure 21 shows the absolute value of outputs relative to the seismic load applied in the longitudinal direction as a parametric modeling case on 65.4 m length and 3.0 m height of backfill considered by backfill stiffness including soil stiffness around the pile. When backfill stiffness is highly subjected to ground motion, the maximum lateral force in the longitudinal direction obtained is 45.01 kN for the case where soil around the pile is hard. For intermediate- and low-stiffness backfill, the same ground motion was applied and the scale included SPI behavior in structural models. The maximum lateral force found for those cases was 49.78 and 46.23 kN, respectively. The difference between maximum displacements obtained from high, intermediate, and low stiffness backfill were 82.26% and 96.87%, respectively (Fig. 21b).

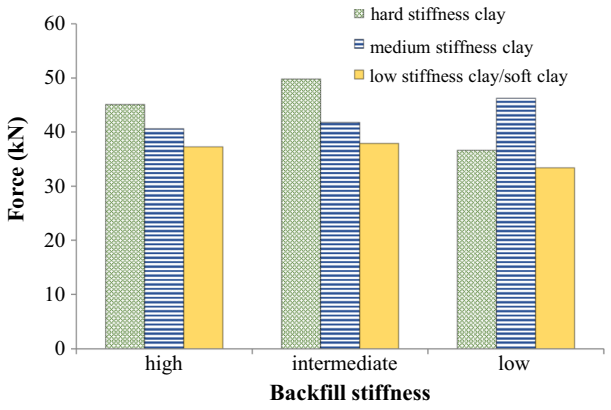

(a) The absolute value of lateral forces

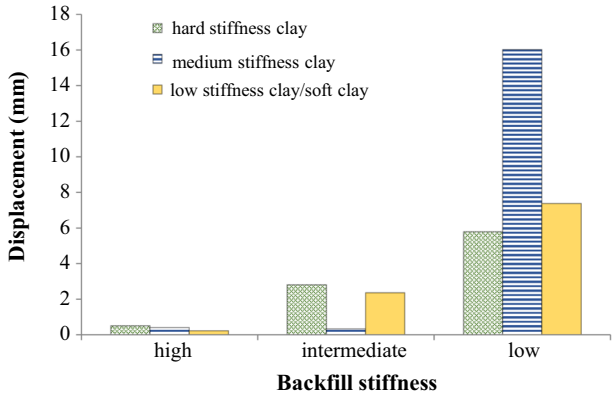

(b) The absolute value of displacements

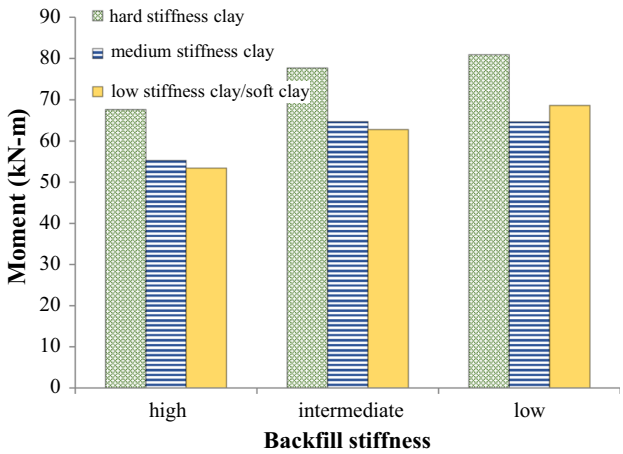

(c) The absolute value of pile head moments

Fig. 21 Effects of soil stiffness around the pile

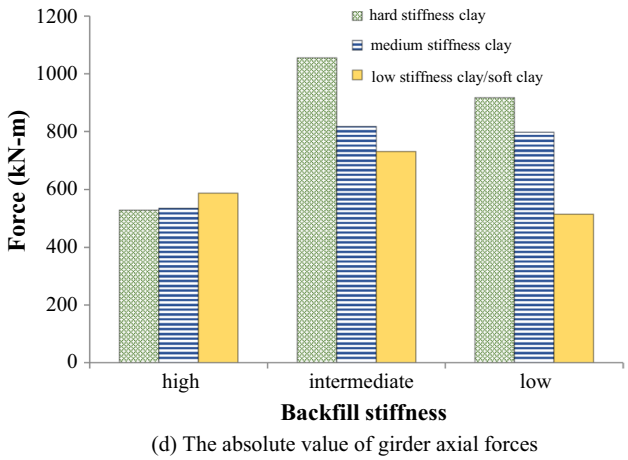

(d) The absolute value of girder axial forces

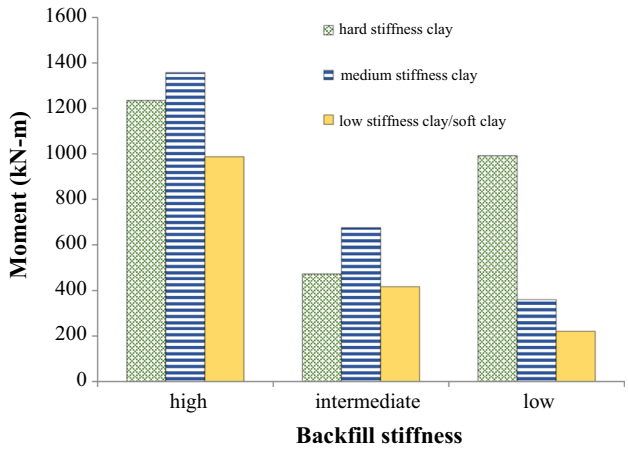

(e) The absolute value of abutment head moments

Fig. 21 (continued)

6 Conclusion

Integral abutment bridge construction is an increasingly common alternative to conventional bridge construction, as it removes expansion joints, bearings and their related maintenance problems. However, in the absence of expansion joints and bearings, the abutments and piles must be capable of accommodating lateral movements of the bridge due to thermal expansion and contraction and seismic movements. The present study developed numerical modeling to investigate seismic analysis and probabilistic simulations of IABs. To validate the numerical modeling, we examined lateral force and dynamic load response to the finite element model process in both static and dynamic conditions. A constructed bridge was selected as an example. A model formulated for a pile was implemented in the bridge to verify software used in this study. Afterward, we examined the *p*–*y* curves of piles at various heights below the ground. As indicated in the NCHRP curve (Barker et al. 1991), there is no distinction in the type of rigid-body movement that generates the displacement measured at the top of the abutment: abutments can experience pure translational, pure rotational, or combined translational-rotational response to generate a top displacement. In this study, we did not consider rotational and translational degrees of freedom. The parametric study consisted of four variables, namely the bridge span (short, medium, and long spans of 18.3, 35.4, and 64.5 m,

respectively), value of the backfill pressure (3.1, 4.6, and 6.1 m, respectively), stiffness of soil mixture backfills (high, intermediate, and low stiffness), and soil density around the piles (high, intermediate, and low). Because of the small width–length ratio of the bridge, a 2D model of IAB with soil springs around the piles and abutments was developed. By applying seismic loading, maximum pile deflection and abutment displacement occurred at the top of the pile where it was connected to the abutment. This deflection is affected by the banded stiffness of sand behind the abutment and the stiffness of clay around piles. IAB was modeled with all the critical details in FEM software. Then, for the defined SSI, *p*–*y* curves were used to verify to the software. The Beam3 element was used for pile, abutment, back wall, and superstructure. Also, the COMBIN39 element was used for nonlinear springs of soil. In subsequent sections, we used AllPile software to obtain the *p*–*y* curve of piles, and then the diagram of force–displacement for abutments was drawn. Finally, the model was formulated, and time history dynamic loads were applied to the bridge. The parametric study considered several parameters (i.e., bridge span, backfill height, backfill stiffness, soil type around piles, and soil stiffness around piles, using three variables of clay stiffness around piles [i.e., high, intermediate, and low] from each parameter, resulting in 81 parametric study cases).

Based on the analytical results, several conclusions were drawn:

- Under seismic loads, the maximum moments in the pile were at the pile–abutment interfaces. The pile moments decreased when abutment backfill was high-stiffness sand and increased when piles were placed in dense clay. Therefore, this moment is greatest for the case with piles in high-stiffness clay and low-density backfill, and smallest for the case with piles in intermediate-stiffness clay around the pile and high-stiffness backfill.
- Bridge span played a significant role in the performance of IAB (i.e., pile lateral forces, pile bending moments at pile head, tensile and compressive girder axial forces, and bending moments at the abutment).
- Backfill height, which is important for the distribution of induced forces transmitted into the soil, should be considered together with other parameters.
- The maximum axial girder moments at the superstructure generally decrease when the combined stiffness of soil behind the abutment and around piles increases, similar to pile deflection and abutment displacement. However, the maximum abutment head moments decreased when abutment backfill was dense and increased when piles were located in hard clay, similar to pile moments.
- Dense sand backfilling behind abutments is recommended, since it decreased the pile deflections, pile lateral forces, abutment displacements, abutment head moments, and in particular pile bending moments.
- Upon evaluating the *p*–*y* backbone curves in relation to depth, it became evident that as depth increased, there was a corresponding increase in soil resistance and a decrease in pile displacement. This observation seems to be due to the fact that the largest shear force is generated at the head of the pile, as a result of the load imposed by the pile cap and the upper structure. Furthermore, it is important to note that soil-structure interaction (SSI) studies are currently limited to issues with similar *p*–*y* curves. Therefore, it is essential to generate individual *p*–*y* curves for each structure.

Funding Open access funding provided by University of Botswana. This research received no specific grant from any funding agency in the public, commercial, or not-for-profit sectors.

Declarations

Conflict of interest The authors declare that they have no competing interests.

References

Abdel-Fattah MT, Abdel-Fattah TT (2019) Behavior of integral frame abutment bridges due to cyclic thermal loading: nonlinear finite-element analysis. J Bridg Eng 24(5):04019031. https://doi.org/10.1061/(ASCE)BE.1943-5592.0001394

Arsoy S, Barker RM, Duncan JM (1999) The behavior of integral abutment bridges. Virginia Transportation Research Council

Abdelrahman A, Tawfik M, El-Saify A (2018) Investigation on the performance of bridge approach slab. In: MATEC Web of Conferences, EDP Sciences. vol 162, p 04014. https://doi.org/10.1051/matecconf/201816204014

Barghian M, Khatibi SK, Hajialilue-Bonab M (2020) Soil behavior around the stub abutment of an integral bridge and buried piles in the contraction state. Sci Iran Trans A Civ Eng 27(1):88–104. https://doi.org/10.24200/SCI.2018.20030

Barker RM, Duncan JM, Rojiani KB, Ooi PS, Tan CK, Kim SG (1991) Manuals for the design of bridge foundations: shallow foundations, driven piles, retaining walls and abutments, drilled shafts, estimating tolerable movements, and load factor design specifications and commentary (No. 343)

Boulanger RW, Curras CJ, Kutter BL, Wilson DW, Abghari A (1999) Seismic soil-pile-structure interaction experiments and analyses. J Geotech Geoenviron Eng 125(9):750–759. https://doi.org/10.1061/(ASCE)1090-0241(1999)125:9(750)

Bigelow H, Pak D, Hoffmeister B, Feldmann M, Seidl G, Petraschek T (2017) Soil-structure interaction at railway bridges with integral abutments. Procedia Eng 199:2318–2323. https://doi.org/10.1016/j.proeng.2017.09.204

Civjan SA, Bonczar C, Brena SF, DeJong J, Crovo D (2007) Integral abutment bridge behavior: parametric analysis of a Massachusetts bridge. J Bridg Eng 12(1):64–71. https://doi.org/10.1061/(ASCE)1084-0702(2007)12:1(64)

Dicleli M (2016) Integral bridges. In: Innovative bridge design handbook. Butterworth-Heinemann, pp 429–450

Frosch RJ, Wenning M, Chovichien V (2005) The in-service behavior of integral abutment bridges: abutment-pile response. In: Integral Abutment and Jointless Bridges (IAJB 2005) Federal Highway AdministrationWest Virginia Department of Transportation

Khosravikia F, Potter A, Prakhov V, Zalachoris G, Cheng T, Tiwari A, Paine J (2018) Seismic vulnerability and post-event actions for Texas bridge infrastructure (No. FHWA/TX-18/0–6916–1). Center for Transportation Research at the University of Texas at Austin

Kwon OS, Elnashai A (2006) The effect of material and ground motion uncertainty on the seismic vulnerability curves of RC structure. Eng Struct 28(2):289–303. https://doi.org/10.1016/j.engstruct.2005.07.010

Kotsoglou A, Pantazopoulou S (2007) Bridge–embankment interaction under transverse ground excitation. Earthq Eng Struct Dyn 36(12):1719–1740. https://doi.org/10.1002/eqe.715

Lesgidis N, Sextos A, Kwon OS (2017) Influence of frequency-dependent soil–structure interaction on the fragility of R/C bridges. Earthq Eng Struct Dyn 46(1):139–158. https://doi.org/10.1002/eqe.2778

Lesgidis N, Sextos A, Kwon OS (2018) A frequency-dependent and intensity-dependent macroelement for reduced order seismic analysis of soil-structure interacting systems. Earthq Eng Struct Dyn 47(11):2172–2194. https://doi.org/10.1002/eqe.3063

Lim H, Jeong S (2018) Simplified py curves under dynamic loading in dry sand. Soil Dyn Earthq Eng 113:101–111. https://doi.org/10.1016/j.soildyn.2018.05.017

Li C, Pan H, Tian L (2022) Seismic performance analyses of pile-supported transmission tower-line systems subjected to depth-varying spatial ground motions. J Earthq Eng. https://doi.org/10.1080/13632469.2022.2113000

Mahjoubi S, Maleki S (2020) Finite element modeling and seismic behaviour of integral abutment bridges considering soil–structure interaction. Eur J Environ Civ Eng 24(6):767–786. https://doi.org/10.1080/19648189.2017.1421483

Makris N, Badoni D, Delis E, Gazetas G (1994) Prediction of observed bridge response with soil-pile-structure interaction. J Struct Eng 120(10):2992–3011. https://doi.org/10.1061/(ASCE)0733-9445(1994)120:10(2992)

Mylonakis G, Nikolaou S, Gazetas G (2006) Footings under seismic loading: analysis and design issues with emphasis on bridge foundations. Soil Dyn Earthq Eng 26(9):824–853. https://doi.org/10.1016/j.soildyn.2005.12.005

Naji M, Firoozi AA, Firoozi AA (2020) A review: study of integral abutment bridge with consideration of soil-structure interaction. Lat Am J Solids Struct. https://doi.org/10.1590/1679-78255869

Nakhaei M, Ghannad MA (2008) The effect of soil–structure interaction on damage index of buildings. Eng Struct 30(6):1491–1499. https://doi.org/10.1016/j.engstruct.2007.04.009

Perić D, Miletić M, Shah BR, Esmaeily A, Wang H (2016) Thermally induced soil structure interaction in the existing integral bridge. Eng Struct 106:484–494. https://doi.org/10.1016/j.engstruct.2015.10.032

Pal AS, Baidya DK (2018) Dynamic analysis of pile foundation embedded in homogeneous soil using cone model. J Geotech Geoenviron Eng 144(8):06018007. https://doi.org/10.1061/(ASCE)GT.1943-5606.0001927

Pugasap K (2006) Hysteresis model based prediction of integral abutment bridge behavior. The Pennsylvania State University

Rahmani A, Taiebat M, Finn WL, Ventura CE (2018) Evaluation of py springs for nonlinear static and seismic soil-pile interaction analysis under lateral loading. Soil Dyn Earthq Eng 115:438–447. https://doi.org/10.1016/j.soildyn.2018.07.049z

Saitoh M (2007) Simple model of frequency-dependent impedance functions in soil-structure interaction using frequency-independent elements. J Eng Mech 133(10):1101–1114. https://doi.org/10.1061/(ASCE)0733-9399(2007)133:10(1101)

Salman NN, Issa MA (2019) Displacement capacities of H-piles in integral abutment bridges. J Bridg Eng 24(12):04019122. https://doi.org/10.1061/(ASCE)BE.1943-5592.0001482

Shamsabadi A, Ashour M, Norris G (2005) Bridge abutment nonlinear force-displacement-capacity prediction for seismic design. J Geotech Geoenviron Eng 131(2):151–161. https://doi.org/10.1061/(ASCE)1090-0241(2005)131:2(151)

Stefanidou SP, Sextos AG, Kotsoglou AN, Lesgidis N, Kappos AJ (2017) Soil-structure interaction effects in analysis of seismic fragility of bridges using an intensity-based ground motion selection procedure. Eng Struct 151:366–380. https://doi.org/10.1016/j.engstruct.2017.08.033

Sextos AG, Pitilakis KD, Kappos AJ (2003) Inelastic dynamic analysis of RC bridges accounting for spatial variability of ground motion, site effects and soil–structure interaction phenomena. Part 1: methodology and analytical tools. Earthq Eng Struct Dyn 32(4):607–627. https://doi.org/10.1002/eqe.241

Shamsi M, Zakerinejad M, Vakili AH (2021) Seismic analysis of soil-pile-bridge-train interaction for isolated monorail and railway bridges under coupled lateral-vertical ground motions. Eng Struct 248:113258. https://doi.org/10.1016/j.engstruct.2021.113258

Shedge HN, Kumar M (2022) Response of perforated H-pile subjected to coupled lateral displacement history and axial loading. Aust J Struct Eng. https://doi.org/10.1080/13287982.2022.2149914

Souri M, Khosravifar A, Dickenson S, McCullough N, Schlechter S (2022) Effects of long duration earthquakes on the interaction of inertial and liquefaction-induced kinematic demands on pile-supported wharves. Soil Dyn Earthq Eng 154:107155. https://doi.org/10.1016/j.soildyn.2022.107155

Taskari O, Sextos A (2015) Probabilistic assessment of abutment-embankment stiffness and implications in the predicted performance of short bridges. J Earthq Eng 19(5):822–846. https://doi.org/10.1080/13632469.2015.1009586

Teguh M, Duffield C, Mendis P, Hutchinson GL (2006) Seismic performance of pile-to-pile cap connections: an investigation of design issues. Electron J Struct Eng 6:8–18. https://doi.org/10.56748/ejse.654

Tam VY, Le KN (2019) Sustainable construction technologies: life-cycle assessment. Butterworth-Heinemann

Wang ST, Reese LC (1993) COM624P-Laterally loaded pile analysis program for the microcomputer, Version 2.0 (No. FHWA-SA-91-048). Federal Highway Administration. Office of Technology Applications, US

Xie Y, DesRoches R (2019) Sensitivity of seismic demands and fragility estimates of a typical California highway bridge to uncertainties in its soil-structure interaction modeling. Eng Struct 189:605–617. https://doi.org/10.1016/j.engstruct.2019.03.115

Xie Y, Huo Y, Zhang J (2017) Development and validation of p-y modeling approach for seismic response predictions of highway bridges. Earthq Eng Struct Dyn 46(4):585–604. https://doi.org/10.1002/eqe.2804

Zhang Y, Conte JP, Yang Z, Elgamal A, Bielak J, Acero G (2008) Two-dimensional nonlinear earthquake response analysis of a bridge-foundation-ground system. Earthq Spectra 24(2):343–386. https://doi.org/10.1193/1.2923925